# Eco-friendly aerosol multicoated silicon anodes in lithium-ion batteries

Pin-Yi Zhao[†‡], Antonio Ruiz Gonzalez [†‡], Bing Li[†]*, Kwang-Leong Choy[†]*

[†]Institute for Materials Discovery, University College London, WC1E 7JE, United Kingdom

[‡]Department of Chemistry, University College London, WC1H 0AJ, United Kingdom

*Corresponding author. E-mail address: k.choy@ucl.ac.uk

**Abstract**

Silicon is a promising alternative anode material in lithium-ion batteries as it has a higher theoretical specific capacity than the commercial graphite-based anodes. Within this work, a new multicoated composite material was fabricated through a simple, non-vacuum, and economical aerosol-assisted chemical deposition. This eco-friendly preparation method was developed for the first time with the sodium alginate for a nano-silicon composite. Such a multicoated composite generates excellent electrochemical performance. Our results suggest that the anode delivers a specific capacity of ~760 mAh $g^{-1}$ at 0.36 A $g^{-1}$ after 300 discharge/charge cycles.

**Keywords:** Eco-friendly; Aerosol-assisted chemical deposition; Lithium-ion batteries; Silicon anodes

## 1. Introduction

The commercialisation of lithium-ion batteries has significantly benefited modern society since their invention thirty years ago [1, 2]. After decades of continued effort, the conventional carbonaceous anode is now reaching its theoretical limit [3]. Alternatively, silicon is investigated due to its remarkable gravimetric specific capacity and low de-lithiation potential [4]. However, the large-scale employment of silicon anodes is still hindered by severe volume inflation and limited electrical conductivity [5].

As a critical aspect of coping with the above limitation, the binder in the batteries can influence the performance of silicon-based materials more than generally perceived [6]. There are two dominant categories of binders: organic-soluble binders (e.g., polyvinylidene fluoride (PVDF)) and water-soluble binders [7]. PVDF demands N-Methyl-2-pyrrolidone (NMP, $T_b = 203$ °C) which is expensive, teratogenic and toxic [8] as the solvent. On the other hand, water-soluble binders (eg., sodium alginate) are eco-friendly alternatives for silicon anodes. Alginate is a polysaccharide molecule rich in carboxyl groups that allows the formation of hydrogels through the complexation of cations and contributes to superior cycling performance [9, 10]. Most of all, alginate could be aqueously processed, thus avoiding toxic, high-cost solvents and contributing to the eco-friendliness and sustainability of the manufacture [11].

In this work, electrodes are fabricated through aerosol-assisted chemical deposition (AACD) [12]. Considering its versatile, low-cost, and promising potential for mass production with uniform structure, composition and thickness control, AACD is developed herein as an eco-friendly process in batteries. The excellent electrochemical performance of the as-prepared material is demonstrated.

## 2. Methods

a. Experimental. The raw materials, equipment, and test methods are provided in the Supporting Information. The aerosol multicoated silicon electrode is denoted as AS.

b. Univariate linear regression. A brief introduction, principle and evaluation metrics are included in the Supporting Information.

## 3. Results and discussion

To determine the presence of carboxyl groups within the surface of the alginate, Fourier-transform infrared spectroscopy (FTIR) was employed over 4000 $cm^{-1}$ to 400 $cm^{-1}$. Figure 1a displays FTIR spectra. The sodium alginate presents hydrogen-bonded stretching vibrations of O-H, featuring ~3320 $cm^{-1}$ of a broad absorption band [9]. Asymmetric vibrations of carboxylate (O-C-O) are shown at ~1598 $cm^{-1}$. The peak concerning symmetric O-C-O vibrations is displayed at ~1410 $cm^{-1}$. The peak of ~1300 $cm^{-1}$ corresponds to the pyranose rings (O-C-H and C-C-H deformation). This peak is much weaker in the electrode (AS) due to the hydrogen bonds between the alginate and the surface of nano-silicon [13, 14]. The peak of ~1028 $cm^{-1}$ corresponds to the asymmetric vibrations of C-O-C. Nano-silicon features an absorption band (Si-O stretch mode) at ~1120 $cm^{-1}$, as well as an absorption band (Si-O-Si wag mode) at ~2250 $cm^{-1}$ [15]. Another absorption band, corresponding to the Si-H bending mode, occurs at ~880 $cm^{-1}$.

To check the wetting property of the ultrapure water on the substrate, the contact angle was measured and presented in Figure 1b. The advancing angle is 80.07° with a hysteresis of 1.78°. The contact angle (~80°) supports that the ultrapure water covers (<90°) the spacer. Therefore, both parties could be considered for good deposition.

A homogeneously heated substrate is necessary for uniform deposition. The thermographic image is adopted to check the homogeneity of the setting. Figure 1c is obtained after thermal equilibrium for the set. As expected, the substrate presents a uniform thermal pattern with a centre of slightly lower temperature than the surroundings. The as-deposited electrodes are demonstrated in Figure 1d with uniform features. The deposited electrodes are robust and cannot be easily scraped from the substrate. Fig. S1 shows the indentation profile of the electrode. The hardness and elastic modulus are comparable with the existing report [16]. The robust assembly may give rise to enhanced cycling stability [17]. Figure 1e displays the thickness of the deposition as the difference of 0.028 mm between the substrate and the electrode.

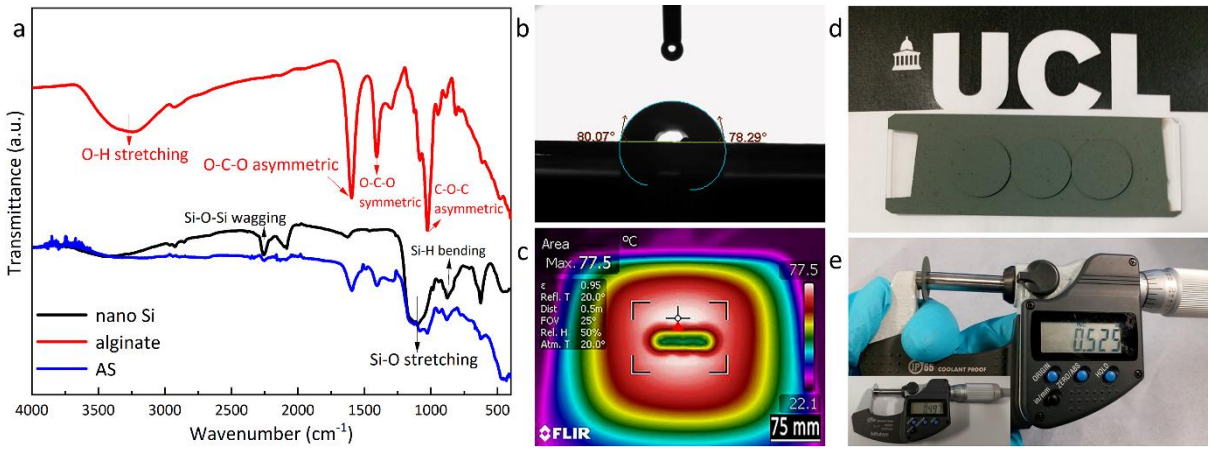


Figure 1 (a) FTIR of nano-silicon, alginate, and the electrode (AS), (b) The contact angle of ultrapure water with the spacer, (c) Thermographic image of the setting, (d) Digital image of the as-prepared electrode deposited by aerosol-assisted chemical deposition, (e) Thickness of the fabricated electrode (with the spacer), and inset (only the spacer)

The morphology of the sample is analysed by scanning electron microscope (SEM) with elemental mapping by the energy-dispersive X-ray spectroscopy (EDS). The sample is micrometre-sized aggregates (Figure 2a) due to nanomaterials' high surface energy [18]. In

addition, the expected composition of the sample is observed in Figure 2b-d. It can be seen from the surface that there is silicon, and sodium elements, therefore proving that nano-silicon particles are mixed with the sodium alginate.

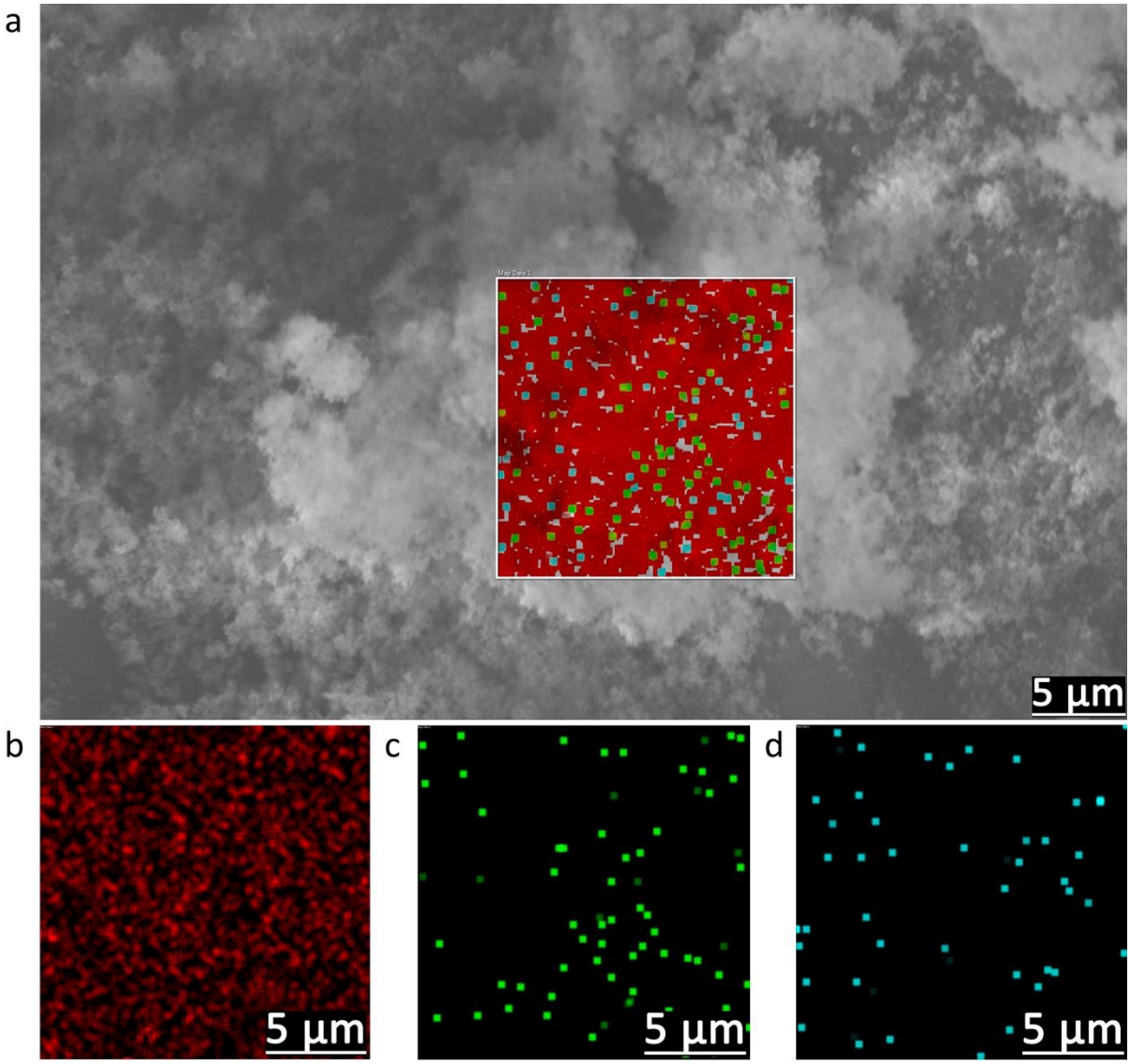


Figure 2 (a) SEM image of the obtained electrode after deposition by aerosol-assisted chemical deposition and EDS elemental mapping of (b) Silicon, (c) Carbon, and (d) Sodium

The electrochemical behaviour of the as-deposited electrode is studied. Redox of the materials is analysed through cyclic voltammetry, as is presented in Figure 3a. The 1$^{st}$ scan exhibits a broad cathodic peak between 0.8 V and 0.4 V, forming the solid electrolyte interface (SEI) [19]. Oxidative signals appear at 0.4 V and 0.54 V with broad peaks. Due to the activation process,

these dealloying peaks develop more distinctly in the following cycles [20]. The 3rd cycle of the scan tends to present the same peak position as the 2nd cycle, implying the favourable reversibility of the electrode [21] after the electrochemical activation.

Galvano electrochemical impedance spectrum (GEIS) from $10^6$ to 0.01 Hz (Figure 3b) is acquired when 100 discharge/charge cycles are finished. Two semicircles and a low-frequency line are observed. The diameter of the semicircle at the high-frequency region is assigned to the charge transfer resistance ($R_{ct}$), noted as R3 (~10 Ω) in the equivalent circuit. Meanwhile, the R2 and C2 refer to the passivating layer's impedance and capacitance, and the 45° straight line at the low-frequency region concerns the solid-state diffusion (Warburg impedance, $Z_w$) [22].

Figure 3c demonstrates the discharge/charge cycling of the electrode under constant-current cycling at 0.36 A $g^{-1}$ (based on the mass of nano-silicon). The specific capacity of the electrode (AS) descends gradually from ~3000 mAh $g^{-1}$ to 760 mAh $g^{-1}$ upon completion of 300 cycles. The severe recession was detected in silicon materials, resulting in an inferior electrochemical performance [23]. This downturn could be ascribed to severe volume alterations, resulting in the electrical disconnection of nano-silicon particles. This cell has a coulombic efficiency of nearly 99 %, but there is a capacity loss every cycle, which is still too severe for practical applications. The generation of unstable solid-electrolyte-interphase (SEI) regularly results in low reversibility, which is the primary cause of poor (initial) coulombic efficiency [24]. The charge curves are laid out in Figure 3d. The shape of the curves is incessant and steady. This figure could be better understood with the ‘fulfilled ratio’ [12], as is shown in Figure 3e. It is calculated that the electrode has accomplished 83.8% of its theoretical limit. Although the very high theoretical specific capacity has been well approached, the capacity retention is still

staggering (26.3%). There could be two reasons for this: (1) a flock of nano-silicon particles and (2) electrolyte additives needed for a stable SEI. The rate performance is shown in Fig. S2. with discussion.

The charge patterns could be further understood as three sections (illustrated in Fig. S3): (1) 0-13%; (2) 13% to 65%; and (3) 65% to 100% of their corresponding specific capacity. The second section is close to linear, while the first section could be transformed to linear by logarithmic transformation. Therefore ~65% in total (first and second sections) of their corresponding specific capacity could be understood via univariate linear regression. Root mean square error (RMSE) and coefficient of determination ($R^2$) of the regression are summarised in Figure 3f and Figure 3g (patterns of the univariate linear regression are presented in Table S1). The RMSE is very close to zero through fivefold cross-validation with predictions on the holdout dataset. Besides, all $R^2$ values are very close to 1, which indicates satisfactory linearity. The results suggest that ~65% specific capacity at the beginning of the charge could be well correlated with the corresponding potential. This promising feature might be applied in battery testing, health monitoring, or lifespan predictions.

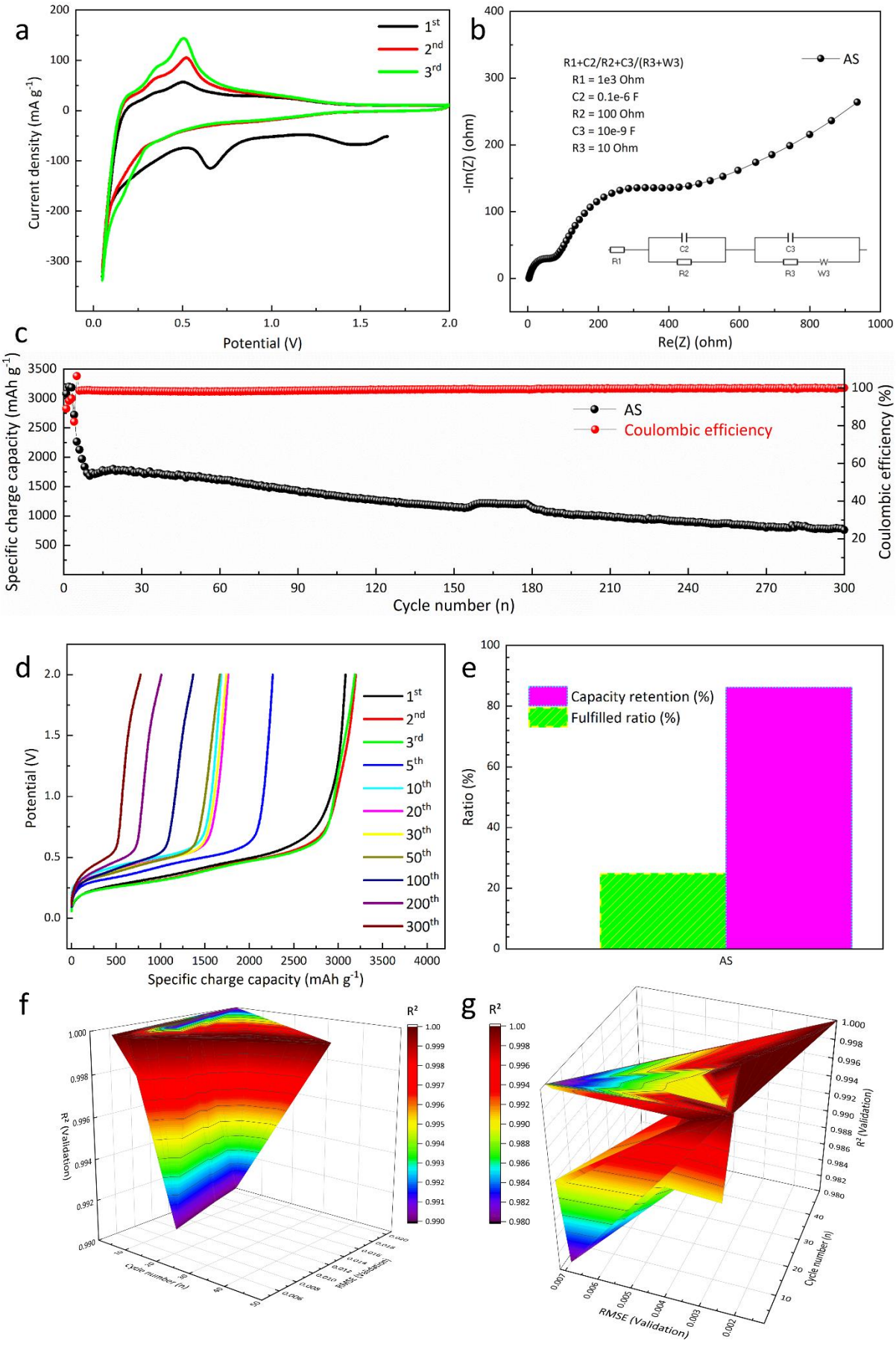
a
Current density (mA g-1)
Potential (V)
1st
2nd
3rd
b
-Im(Z) (ohm)
Re(Z) (ohm)
AS
R1+C2/R2+C3/(R3+W3)
R1 = 1e3 Ohm
C2 = 0.1e-6 F
R2 = 100 Ohm
C3 = 10e-9 F
R3 = 10 Ohm
R1
C2
R2
C3
R3
W
W3
c
Specific charge capacity (mAh g-1)
Coulombic efficiency (%)
Cycle number (n)
AS
Coulombic efficiency
d
Potential (V)
Specific charge capacity (mAh g-1)
1st
2nd
3rd
5th
10th
20th
30th
50th
100th
200th
300th
e
Ratio (%)
Capacity retention (%)
Fulfilled ratio (%)
AS
f
R²
R² (Validation)
Cycle number (n)
RMSE (Validation)
g
R²
R² (Validation)
Cycle number (n)
RMSE (Validation)

Figure 3 (a) Cyclic voltammetry of the electrode conducted at 0.1 mV $s^{-1}$ from 0.05 to 2 V, (b) GEIS of the electrode from $10^6$ to 0.01 Hz with alternating current of 0.1 mA, equivalent circuit inset with parameters, (c) Cycling performance at 0.36 A $g^{-1}$ from 0.05 to 2 V, (d) charge curves of the electrode, (e) corresponding capacity retention and fulfilled ratio, as well as (f) RMSE (validation), $R^2$ (validation) presented in 3D colourmap (with projection) of the first section, and (g) The second section of the charge curves

## 4. Conclusions

To sum up, we have constructed eco-friendly anodes via aerosol-assisted chemical deposition. The anode indicates excellent electrochemical performance (eg., 760 mAh $g^{-1}$ after 300 cycles, with a fulfilled ratio of 83.8%). Considering the eco-friendly synthesis and the promising performance, it would be appealing for electrode materials previously processed with toxic NMP to consider this novel, green approach for laboratory tests in rechargeable lithium-ion batteries. Meanwhile, the material's feature of charge curves is studied via univariate linear regression. The revealed linearity might be utilised in battery testing or health monitoring.

## Acknowledgement

There was no external funding for this study. The support of nano-indentation from Anton Paar is gratefully acknowledged. Thanks to Dr. Yohan Dall'Agnese for his discussion of the manuscript.

## Declaration of competing interest

The authors declare that they have no known conflicting financial interests or personal relationships that would seem to have influenced the work presented in this work.

## References


[1] M.S. Whittingham, Nano Letters 20 (2020) 8435-8437.
[2] J. Liu, et al., Nature Energy 4(3) (2019) 180-186.
[3] S. Chae, et al., Angewandte Chemie International Edition 59(1) (2020) 110-135.
[4] K. Feng, et al., Small 14(8) (2018) 1702737.
[5] P. Li, et al., Energy Storage Materials 35 (2021) 550-576.
[6] J.T. Li, et al., Advanced Energy Materials 7(24) (2017) 1701185.
[7] Y. Ma, et al., Energy Storage Materials 20 (2019) 146-175.
[8] D. Bresser, et al., Energy & Environmental Science 11(11) (2018) 3096-3127.
[9] I. Kovalenko, et al., Science 334(6052) (2011) 75-79.
[10] M.H. Ryou, et al., Advanced materials 25(11) (2013) 1571-1576.
[11] S.-L. Chou, et al., Physical Chemistry Chemical Physics 16(38) (2014) 20347-20359.
[12] P.-Y. Zhao, et al., Materials Advances (2022), DOI: 10.1039/D1MA01007G
[13] R.Z.A. Manj, et al., Chemical Engineering Journal 385 (2020) 123821.
[14] W. Luo, et al., Advanced Energy Materials 7(24) (2017) 1701083.
[15] M.R. Scriba, et al., Thin Solid Films 517(12) (2009) 3484-3487.
[16] P.K. Alaboina, et al., Electrochimica Acta 258 (2017) 623-630.
[17] G. Zhu, et al., National science review 8(6) (2021) nwaa152.
[18] H. Li, et al., Electrochimica Acta 120 (2014) 96-101.
[19] R. Patil, et al., ACS omega 6(10) (2021) 6600-6606.
[20] Z. Luo, et al., Carbon 98 (2016) 373-380.
[21] J. Yu, et al., Applied Surface Science 548 (2021) 148944.
[22] Y. Dall'Agnese, PhD thesis, Drexel University, 2016.
[23] J. Saint, et al., Advanced Functional Materials 17(11) (2007) 1765-1774.
[24] F.-Z. Zhang, et al., Rare Metals 41(4) (2022) 1276-1283.